Proceedings of the 1998 ASME International Congress and Exhibition
Anaheim, CA, Nov, 1998

HYDROFOIL DESIGN AND OPTIMIZATION FOR FAST SHIPS

Eric Besnard, Adeline Schmitz,
Kalle Kaups, and George Tzong
Research Associates

Aerospace Engineering Department
California State University, Long Beach
Long Beach, CA, 90840
Tel: (562) 985 5579 • Fax: (562) 985 1669
besnarde@csulb.edu • schmitz@csulb.edu

Hamid Hefazi, Orhan Kural,
Hsun Chen, and Tuncer Cebeci
Professors

Aerospace Engineering Department
California State University, Long Beach
Long Beach, CA, 90840
Tel: (562) 985 1503 • Fax: (562) 985 1669
hefazi@csulb.edu • kural@csulb.edu
hhchen@csulb.edu • cebeci@csulb.edu

ABSTRACT

The paper presents a multi-disciplinary design/optimization method for the conceptual design of a hydrofoil based fast ship. The method is used to determine the maximum achievable lift-to-drag ratio (L/D) of an isolated foil-strut arrangement (hopefully greater than 50) at high transit speeds (greater than 75 knots) while lifting masses of 5,000 and 10,000 tons. First, the tools necessary for the study are presented. They comprise a panel method to compute three-dimensional flows around arbitrary configurations with a model for the free surface, a foil cross-section optimization tool, a strut cross-section design tool, and a structural analysis tool. The computational tools are then integrated into a multi-disciplinary design/optimization approach, which is applied to the design of single foil and biplane configurations. Results show that the goal of L/D = 50 is achievable for 75 knots (assuming that techniques can be developed for reducing the skin friction drag to a quarter of its nominal value) and, that for 90 knots, L/D ratios around 45 can be reached. The corresponding break horsepower requirements for 10,000 tons are around 130 khp and less than 200 khp, respectively.

1 INTRODUCTION

The paper presents a method for the conceptual design of a hydrofoil based fast ship (Fig. 1). The objective is to reduce drastically unrefueled sea lift transit times to remote locations (e.g. from North America to the Middle East) by reaching cruise speeds around 100 knots (1 knot = 0.5150 m/s). The essential factor in attaining a range of at least 10,000 nautical miles (1 nautical mile = 1.854×10^3 m) is the determination of the maximum practical lift-to-drag ratio, consistent with the desired high speed limits set by cavitation onset and structural considerations.

The paper concentrates on a single lifting surface carrying up to 10,000 metric tons of mass above the sea surface and having a maximum span of 65 meters (limited by Suez Canal). Stability and control are not investigated here.

The objective of the study is to determine the maximum achievable lift-to-drag ratio (L/D) of an isolated foil-strut arrangement (hopefully greater than 50) at high transit speeds (greater than 75 knots) while lifting masses of 5,000 or 10,000 tons.

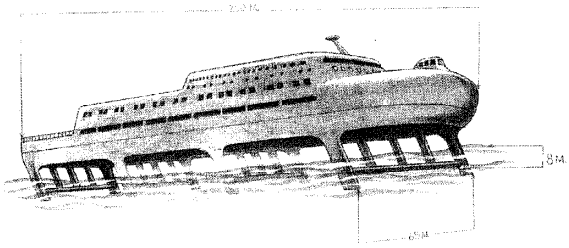

Figure 1. Artist concept of fast ship.

The design method is presented in Sect. 2. First, the tools needed in the design approach are presented in Sects. 2.1 to 2.4. They comprise a panel method to compute three-dimensional flows around arbitrary configurations, a foil cross-section optimization tool, a strut cross-section design tool, and a structural analysis tool. These tools are integrated into a multi-disciplinary design/optimization process in Sect. 2.5.

Section 3 presents results for a single foil configuration. The effects of foil sweep (to increase foil thickness), structural reinforcements (to increase local strength), and endplates (to reduce induced drag) are analyzed. Several points in the design space are considered for speeds of 75 and 90 knots, and masses of 5000 and 10000 tons.

Also, a biplane configuration is investigated in Sect. 4 to determine whether a more sound structural arrangement could lead to substantial improvements. Preliminary results are shown and compared with those obtained for the single foil configuration.

The paper ends with a short description of the design method and a summary of the more important conclusions. Finally, in light of these conclusions, directions for further research are outlined.

2 DESIGN METHOD

This section presents the method used to design the hydrofoil-strut assembly. First, the necessary tools are presented. The calculation method used for three-dimensional flow calculations with the free surface modeled by negative image is presented in Sect. 2.1, along with a sample test case. Then, the design of foil and strut cross-sections is presented in Sect. 2.2 and 3.3, respectively. The tools and hypothesis used for structural analysis are presented in Sect. 2.4. These tools are integrated into a multi-disciplinary design procedure in Sect. 2.5.

2.1 Three-dimensional flow predictions

2.1.1 Calculation method

The three-dimensional flow calculations are based on the higher order panel method of Hess et al. (1985) applicable to arbitrary configurations. A configuration (e.g. Fig. 2) is first divided into sections (e.g. wing, body). Each section is defined by a surface grid constituted of panels. All panels are assigned an independent source distribution, while those on a lifting section are assumed to carry a bound vorticity as well. In the calculations, the vorticity is replaced by an equivalent dipole distribution (see e.g. Hess, 1974). The variation of this bound vorticity in the streamwise direction is assumed, while its variation in the spanwise direction is adjusted to satisfy the Kutta condition at the trailing edge. The Kutta condition adopted here assumes equal lower and upper surface pressures at the trailing edge.

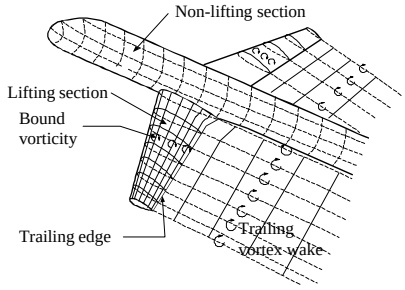

Figure 2. Typical lifting configuration.

The complete solution for a prescribed flow condition is obtained by simultaneously satisfying a condition of zero normal velocity at a control point on each panel of the body together with a Kutta condition at each trailing-edge panel. The fluid velocities and pressures may then be calculated both off and on the body.

The induced drag is evaluated by calculating the energy in the wake by a far-wake procedure known as Treffz-plane analysis (see Durand, 1934). Alternatively the calculated pressures may be integrated over the body panels to give the component of force in the free stream direction. In the limit of a large number of panels these two approaches converge to the same value.

In the case of a hydrofoil, the flow must satisfy a condition of zero (atmospheric) pressure along the free surface. If disturbances are assumed small, i.e. the velocity at the free surface is not very different from its free stream value V and free surface height and slopes are small, the free surface condition may be linearized to

$$V^2\phi_{xx} + g\phi_z = 0 \quad \text{on} \quad z = 0 \tag{1}$$

where g is the acceleration of gravity, and ϕ is either the total potential or the perturbation potential. When the velocity V is large (as is the case here), i.e. the Froude number is large, the free surface can be modeled by negative images, as depicted in Fig. 3, so that the horizontal perturbation velocities cancel out on z = 0.

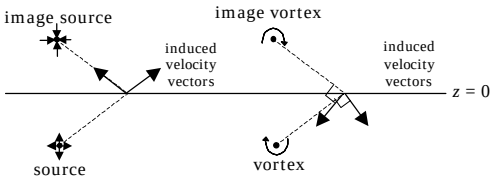

Figure 3. Induced velocities with negative image.

2.1.2 Induced drag and load distribution

For a single wing without winglets in free air, or equivalently at infinite depth in water, the optimum load distribution is elliptic and the corresponding induced drag coefficient is given by

$$C_{Di} = \frac{C_L^2}{\pi A e} \tag{2}$$

with the efficiency factor, e, equal to 1.

The induced drag can be reduced by adding winglets. For hydrofoil applications, struts linking the foil to the boat hull need to be employed, and if the structural requirements imply a "large" number of struts, say greater or equal to 3, it might be beneficial to use these struts as winglets. Figure 4 shows the benefit of adding end-struts to a foil with a rectangular planform. When no end-struts are used, the efficiency factor for the rectangular foil is, as expected, slightly less than 1. With relatively small end-struts, the efficiency factor rapidly increases to values greater than 1.

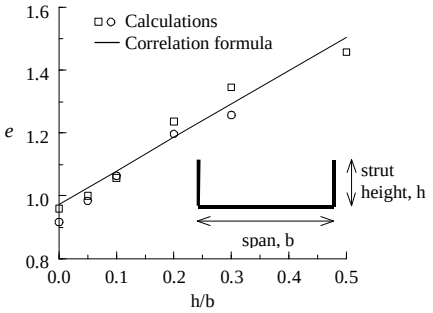

Figure 4. Efficiency factor, *e*, for foil/end-strut configuration at *infinite* depth.

The benefits of having end-struts remain at finite depth (free surface modeled by negative image). The induced drag, however, is drastically increased, as depicted in Fig. 5. For example, struts with d/b = 0.3 are required to reach an efficiency factor corresponding to elliptic loading (e = 1).

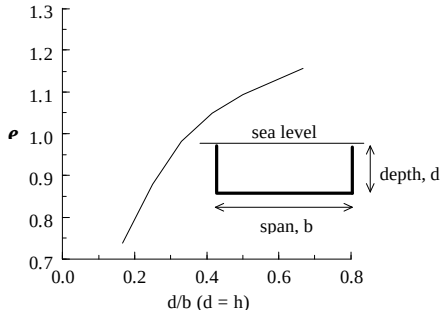

Figure 5. Efficiency factor, *e*, for foil/end-strut configuration at *finite* depth.

Figure 6 shows a typical variation of the load along the foil span and along the struts for a U-shaped configuration (strut chord equals to foil chord and the strut does not extend below the foil). C_n is the normal force coefficient, c the local chord and $\bar{c}$ the average foil chord (equal to c here). The load on the foil is almost constant up to the junction. It is continuously transferred to the strut, drastically diminishes when getting closer to the surface, and goes to zero at the free surface.

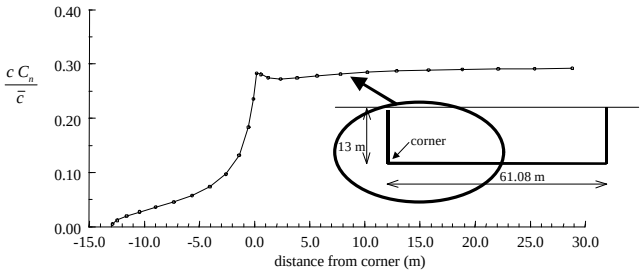

Figure 6. Load variation for the U-shape foil-strut configuration.

2.2 Hydrofoil cross-section design/optimization

When the pressure on the upper surface of the airfoil reaches vapor pressure, i.e. when the local $C_p = -\sigma_i$ (σ_i is the cavitation index), the foil cavitates and drag is drastically increased.

Cavitation inception depends on the speed and depth at which the foil is operating. A family of cavitation-free profiles which maximize lift (thus minimize the required lifting area) for the cavitation indexes corresponding to various combinations of speed and depth needs to be designed. For a given cavitation number, there is an infinite number of profiles that are cavitation free with the thinner ones leading to higher lift and lower drag coefficients. Unfortunately, the structural strength of the configuration depends directly on the foil thickness and thickness variations must be considered.

A two-dimensional optimization is implemented to find the "best" cavitation-free profile (maximum lift) for a given maximum thickness-to-chord ratio (t/c). The optimization process is explained in details in Besnard et al., (1998b). For a chosen σ_i, it allows to determine, at a given t/c, the highest (two-dimensional) lift coefficient at which a foil with can operate and to calculate the resulting drag (friction + form). Also the foil is designed so that there is no flow separation, which would otherwise also greatly increase the drag.

For the application to hydrodynamic optimization, the three main components of the numerical method are, (1) the representation of a configuration by a set of design variables, (2) the optimization method, and (3) the evaluation of hydrodynamic performance of the given configuration. For the present problem, the design variables are shape function coefficients described in Sect. 2.2.2 which represent the foil geometry. The objective function is the lift coefficient calculated using an Interactive Boundary Layer approach discussed in Sect. 2.2.3. The constraints are related to cavitation, thickness ratio and flow separation.

2.2.1 Optimizer

In the present study, the optimizer used is a commercially available optimizer DOT (Vanderplaats et al., 1994), based on the method of Modified Feasible Directions (MFD). All gradients are calculated by finite difference.

2.2.2 Design variables to represent airfoils

To perform the optimization, one must be able to represent a general shape by a finite set of functions. Upper and lower surfaces of an airfoil can be represented by

$$y(\bar{x}) = y_0(\bar{x}) + \sum_{i=1}^{s} x_i \; f_i(\bar{x}) \qquad (3)$$

where x is the coordinate along the airfoil chord, y_0 is a reference airfoil, e.g. a NACA 0012 airfoil, $(x_i)_{1\le i\le s}$ are the design variables, and $(f_i)_{1\le i\le s}$ are the base functions. Several types of base functions can be used. Hicks-Henne functions have been chosen because they allow for a greater local control on the foil shape (Hicks and Henne, 1978, and Eyi, 1995).

2.2.3 Interactive Boundary Layer (IBL) approach for performance predictions

For a given configuration, the flow field can be calculated by either solving the Navier-Stokes (NS) equations or employing an Interactive Boundary Layer (IBL) approach, which is based on the interactive solution of the inviscid and boundary layer equations. While the latter is not as general as the former, it offers a good compromise between the efficiency and the accuracy needed in a design environment and is therefore selected here. Also, for the purpose of hydrofoil design subject to low cavitation numbers, Reynolds numbers are large, viscous effects are small and therefore the boundary layer approximation is appropriate. For the present application, results with the IBL approach are as accurate as with NS methods.

The IBL method has been used extensively for single and multi-element airfoil flow field predictions and is described in greater detail in previous publications (e.g. Cebeci et al., 1996, and Besnard et al., 1998a). The two-dimensional profile drag (friction + pressure drag) is calculated several chords downstream of the trailing edge with the Squire-Young formula (Squire and Young, 1938).

If the skin friction is reduced to ½ or ¼ of its nominal value, the pressure drag is also reduced to ½ and ¼, respectively. This means that the profile drag results can be divided by 2 or 4 to account for a reduced skin friction.

The design optimization approach has been successfully implemented for several high lift applications including inverse design (pressure matching), optimization of the maximum lift coefficient of airfoils by varying its shape, and maximization of the L/D ratio of multi-element airfoils by adjusting their relative positioning (Besnard et al., 1998a).

The next paragraph presents results obtained for hydrofoil design.

2.2.4 Application to hydrofoils for various cavitation indexes

The optimization method is applied here to the design of foils for cavitation indices between 0.15 and 0.6, for different thickness ratios. Those two limits for the cavitation index correspond to 100 knots, 10 meters depth, and 50 knots, 10 meters depth, respectively.

For each cavitation index, there is a maximum t/c that can be reached, corresponding to the appearance of cavitation on the lower surface of the foil. When the speed increases, or the depth diminishes, the maximum thickness achievable gets smaller. Fortunately, at 100 knots, 10 m the maximum thickness attainable is still around 5% which may be "reasonable" for structural considerations.

Figures 7 and 8 show a sample of profiles and pressure distributions designed for σ_i = 0.267 and various thickness ratios using the optimization method of Sect. 2.2.3. The upper surface changes very little with increased thickness because the pressure distribution is limited by the no-cavitation criterion. Only the lower surface changes with the imposed t/c. For the thickest foil (t/c = 8.5%), the maximum negative pressure on the lower surface reaches values close to the cavitation index. Cavitation will occur on the lower surface for a slightly thicker profile.

Figures 9 and 10 shows the lift and drag coefficients for the entire range of cavitation indices studied and for two Reynolds numbers (60×10^6, 100×10^6). The drag coefficient depends very little on lift coefficient because the pressure distribution is very similar from one profile to another. Therefore, drag mostly depends on foil thickness and Reynolds number. Correlation can be derived to predict lift and drag coefficients as a function of thickness ratio, cavitation index, and Reynolds number, and are represented by continuous lines in Figs. 9 and 10.

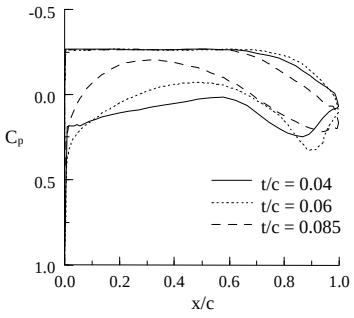

Figure 7. Pressure distribution for optimized foil at σ_i=0.267.

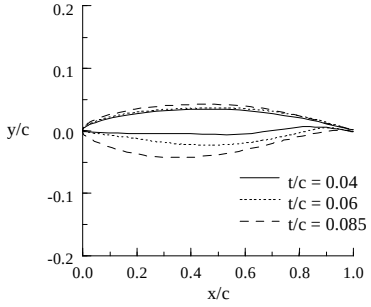

Figure 8. Profile of optimized foil at σ_i=0.267.

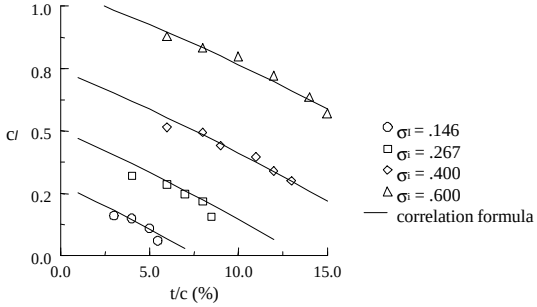

Figure 9. Lift coefficient for different cavitation indices.

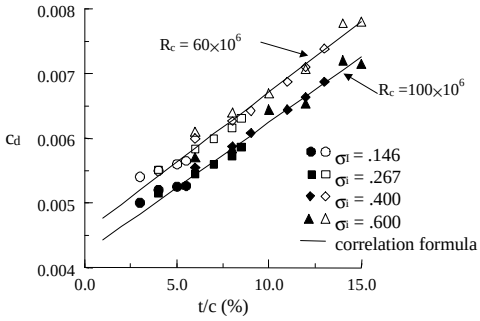

Figure 10. Drag coefficient different cavitation indices.

Note that results are shown without free surface effects. For the depth to chord ratios considered, the presence of the free surface slightly decreases the pressure coefficient on the foil upper surface. This effect being small and conservative, it has been ignored in the present calculations.

2.3 Strut cross-section design

For conceptual design purposes, there are too many unknowns and approximations to design optimized strut profiles for different speeds. The cavitation index of the struts varies from the sea surface to the depth chosen for the foil. Therefore, the thickness ratio of the struts should vary from top to bottom. Also for the faster speeds (75 knots and over), the cavitation-free profile would become very thin near the sea surface. It might then be more advantageous to choose base vented struts or super-cavitating profiles. Also, as previously mentioned, profile drag is almost independent of the airfoil shape and depends primarily on the thickness ratio and the chord Reynolds number.

Therefore, an existing family of symmetrical profiles (The NACA 16-series airfoils) is used for the struts. They have a low maximum velocity (v_{max}), only slightly higher than ellipses ($v_{\max} = 1 + t/c$). The family has approximately a linear variation of the square of the maximum velocity with t/c in the range $6\% \le t/c \le 16\%$. Since $\sigma_i = -C_p \equiv -1 + v_{\max}^2$, σ_i will also be a linear function of t/c.

For a chosen cavitation index, the corresponding airfoil thickness is calculated. Then, the airfoil ordinates are determined using the NACA 16-series equations (Abott and Von Doenhoff, 1959) and the profile drag coefficient is calculated with the IBL code. It is expected that if drag coefficients were minimized using the optimization method used for foil design, the drag reductions compared to the NACA 16-series airfoils would be small, since pressure distribution and foil thickness would be very similar.

Figure 11 shows the variation of thickness ratio with cavitation index for the NACA 16-series struts. Figure 12 presents the strut drag coefficients obtained for t/c varying from 6% to 16%, and R_c of 60×10^6 and 100×10^6. Similarly to the foil, correlation laws can then be derived from Figs. 11 and 12 to predict the profile drag as a function of thickness ratio and Reynolds number. Also for this study, a cavitation index corresponding to mid-depth has been chosen to estimate strut cross-section thickness ratio and drag coefficient.

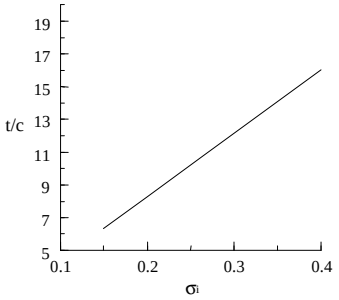

Figure 11. Thickness ratio in function of the cavitation index.

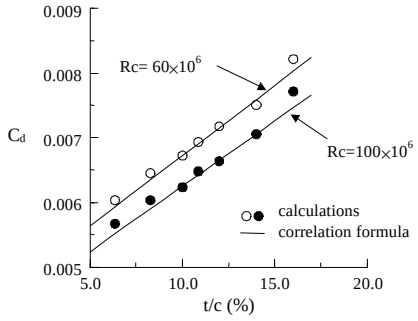

Figure 12. Drag results for NACA 16-series.

2.4 Structural analysis

Structural analysis is necessary to determine the hydrofoil-strut layout for optimum performance (L/D). The struts introduce substantial drag forces to the ship. Hence, it is desirable to minimize the number and sizes of struts. Tradeoffs among design parameters such as the number of struts, wing and strut foil dimensions, and wing span need to be studied in order to optimize the lift-to-drag ratio.

The hydrofoil-strut configuration is modeled by a multi-bay frame as shown in Fig. 13. The structure can be reinforced at certain locations, such as joints between wing and strut and struts themselves (Fig. 14), where higher strength is required.

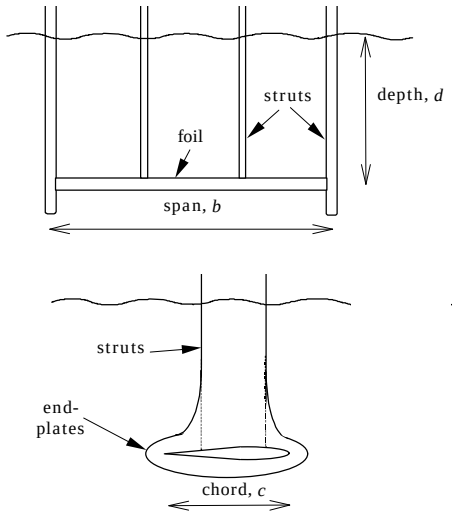

Figure 13. Multi-bay foil-strut assembly.

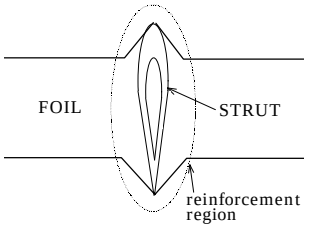

Figure 14. Reinforcement at foil-strut joint.

The structural analysis is based on a FE method and determines the structural design parameters, including foil and strut dimensions, and number of struts. In order to perform quick trade study of those parameters, the wing and struts are approximated by bending beam elements with section properties computed by a simplified geometry with a uniform skin thickness. The simplification retains important structural behaviors of the foil-strut assembly and provides reasonable data for the structural performance evaluation.

2.4.1 Finite element modeling

Finite element (FE) modeling of the foil and strut assembly starts with information of foil dimensions, i.e., chord and t/c, and wing span resulting from hydrodynamic analysis. Both wing and strut cross-sections are modeled by single cell box-type beams as shown in Fig. 15. The chord and t/c for wing and struts can be different. In order to represent the foils with a rectangular box for structural analysis, the width of the beams is approximated by using 75% of chord length. The height of beams is chosen as 85% of the cross-section thickness. The skin thickness of the box is chosen to be uniform with a magnitude not to exceed 50% of the beam height. Using a single-cell box minimizes the number of design parameters and therefore the effort in selecting the optimal structural layout with reasonable accuracy. The configuration of the FE model is shown in

Fig. 16. The small circles indicate the locations of nodal points and a beam element is assigned between two neighboring points. Multiple elements are used to model the foil span between struts and along each strut. The model has an equal bay length between struts. A Y-shape connection between the struts and the ship bottom is used to increase the lateral-load resistance of the struts. Different cross-section properties are assigned to the model depending on the reinforcements and their locations. A computer program generates the finite element model automatically.

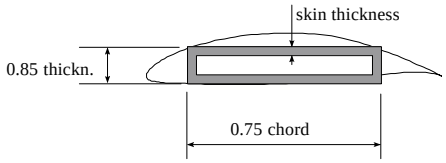

Figure 15. Approximation of foil by a single-cell box for structural analysis.

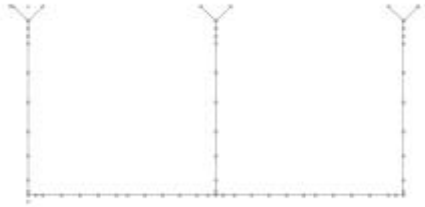

Figure 16. Finite element model of wing-strut assembly.

2.4.2 Load distribution and boundary conditions

Only the strength design of the foil- strut assembly is considered in the study. Three types of loads dominate the strength design: the vertical loads (defined by the weight and payload of the ship), the lateral loads (simulating a combination of critical side crushing waves and high speed turning of ship), and the drag forces. A safety factor of 200% is used for the vertical loads. The lateral loads are chosen to be 50% of the vertical loads and are modeled as concentrated forces applied on the struts at 60% of water depth. The drag forces, with a 500% factor of safety, are estimated based on foil geometry. The drag forces are applied at the same locations as the lateral loads but in the streamwise direction. A uniform distribution of vertical loads on the wing is assumed. The distributions of lateral loads and drag forces among struts are proportional to the amount of vertical loads carried by each individual strut. Figure 17 shows the various loads applied to the foil-strut assembly.

A rigid connection between the struts and the bottom of ship is assumed, as well as between the foil and struts.

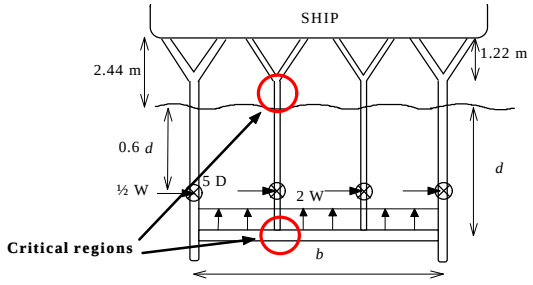

Figure 17. Loads applied to the foil-strut assembly.

2.4.3 Structural analysis

Structural design criteria include the bending strength of the foil, the combination of bending and axial strength of the struts, and overall structural buckling of the foil-strut assembly. The overall buckling load is approximately 30 times higher than the applied load and is therefore not a design concern. The structural internal forces resulting from drag forces are also minor. The dominant design criteria are therefore the bending force on the foil and the combined bending and axial force on the struts due to vertical and lateral loads. It is also found that the axial stresses in the struts are only a small fraction (less than 5%) of maximum stresses. In order to efficiently conduct trade studies, bending forces are used as the safety index to adjust foil and strut dimensions, and the span between struts.

Because the bending forces vary along the foil span and the struts, it is advantageous to use larger chords at critical locations on foil and struts, and smaller chords for under-stressed regions. This selection of chords requires evaluations of results from structural analysis, modification of the FE model and submission of a new computer run for the next analysis. The selection process is repeated until the bending strength is satisfied everywhere on the foil and the struts.

Steel is selected for its high strength as the structural material. Results presented in the following sections are based on steel with an allowable stress of 380 Mpa or 55 ksi.

The distributions of bending moments are different between cases with and without lateral loads as shown in Figs. 18 and 19. Figure 18 shows the moment distribution on a three-strut wing for the case of vertical loads only. Figure 19 includes the distribution on the same configuration with both vertical and lateral loads. The two moment diagrams are quite different from each other. The inclusion of lateral loads has a large impact on the strut strength. It makes the moments at the joints between the foil and the strut and the moment at the Y joints critical (see Fig. 17). Since the lateral loads can be applied from either side of the ship, the structure must be designed symmetrically with respect to its centerline.

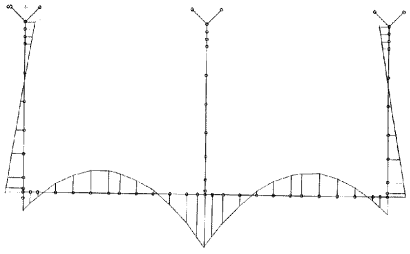

Figure 18. Moment distribution due to vertical loads only.

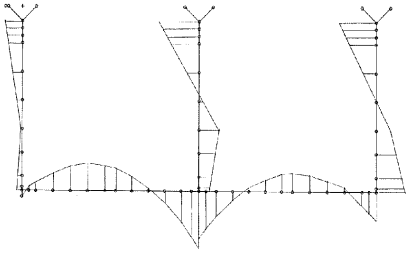

Figure 19. Moment distribution due to both vertical and lateral loads.

2.5 Multi-disciplinary design approach

The design approach presented in this section can be used for conducting parametric studies, or it can be incorporated into a global optimization process. All results presented in the paper are based on the former.

The design is analyzed for *fixed speed and weight* (mass), i.e. the optimum design for that speed-weight combination is the one which provides the maximum L/D and is cavitation free, though it is likely to be right at the limit of cavitation.

For fixed speed and weight, three *global* design variables can be identified:

- depth, d
- foil maximum thickness ratio, (t/c)
- aspect ratio, A

Other design variables exist, e.g. foil skin thickness for structural analysis, but are considered local design variables since they can be adjusted independently of the others. With the three global design variables, the procedure of Fig. 20 is used to generate the configuration and calculate its drag.

First, given weight and speed, select a depth (first independent design variable). The cavitation index is then known. From foil cross-section optimization results for that cavitation index, select a feasible foil maximum thickness ratio (second independent design variable) such that the flow is cavitation free and obtain the corresponding section lift coefficient (two-dimensional).

Then, from typical three-dimensional flow calculations for strut-foil configurations, a corresponding three-dimensional lift coefficient can be determined. For all calculations reported here, it was assumed that the section lift coefficient determined above could be obtained at all spanwise stations. If a rectangular planform is used, minor modifications to the foil cross-section would have to be made near the strut-foil junction in the detailed design.

The foil area can then be determined from

$$S = \frac{M\,g}{\frac{1}{2}\rho V^2 C_L} \tag{4}$$

and selecting an aspect ratio $(A = b^2/S)$ enables to determine the chord and the span of the foil.

At this point, the lifting section of the configuration is entirely known. The induced drag can then be determined as described in Sect. 2.1 (Fig. 5), assuming that there are struts at the tips of the foil. Also, the chord Reynolds number can be calculated and the foil profile drag coefficient is obtained from results of the CFD code of Sect. 2.2 (Fig. 10).

For preliminary calculations, an average strut maximum thickness ratio is determined based on the cavitation index at mid-depth, as described in Sect. 2.3.

A number of struts is selected. Their characteristics (chord, skin thickness, etc.) are also chosen. A structural analysis is then performed as described in Sect. 2.4 to determine the maximum loads vs. the maximum allowables. The structure is then adjusted and subsequent structural analysis performed, until the strut area reaches a minimum while not exceeding the maximum allowables. This structural design process is described in Sect. 2.4 and enables to obtain the minimum number of struts and their local chord.

The corresponding local Reynolds number can be determined at each strut cross-section and the profile drag results of Sect. 2.3 are integrated to obtain the profile drag coefficient of all struts.

The total drag coefficient is then obtained by adding induced drag and foil and strut profile drag:

$$C_D = C_{Di} + \varepsilon\left(C_{Df} + C_{Ds}\right) \tag{5}$$

where C_{Df} and C_{Ds} are the foil and strut profiles drag coefficients, respectively. Here $\varepsilon = 1$ for the nominal drag coefficient, $\varepsilon = 0.5$, or 0.25 if skin friction reduction can be obtained. The resulting lift-to-drag ratio is then calculated along with the maximum (at the start of cruise) Break Horse Power (BHP given in hp and 1hp = 0.7457×10^3 W) requirement which is given by

$$BHP = 6.7654\frac{W_{(\text{metric tons})}\;V_{(\text{knots})}}{\eta_p\;L/D} \tag{6}$$

where $\eta_p = 0.75$.

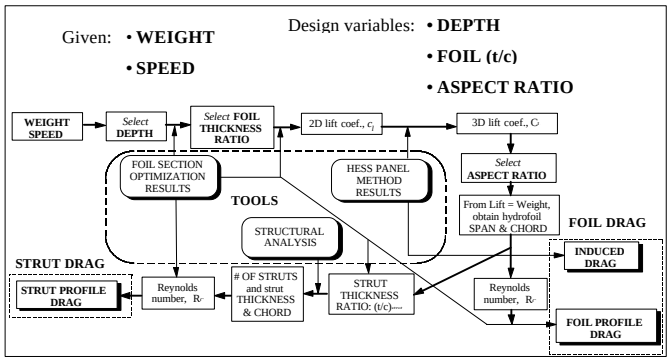

Figure 20. Design approach.

3 RESULTS FOR SINGLE FOIL CONFIGURATIONS

The approach of Sect. 2.0 is applied here to the single foil configuration shown in Fig. 13. Preliminary results and design improvements are first discussed in Sect. 3.1. The relevant improvements are then incorporated into the design process and results are shown for a variety of configurations in Sect. 3.2.

3.1 Preliminary L/D results and design improvements

The design approach of Sect. 2.0 was applied to the single foil configuration and design variables were varied to determine achievable lift-to-drag ratios. Since the L/D values were too low (less than 40 with quarter skin friction for 75 knots), modifications had to be made to the design. In order to reduce the drag, three main improvements were considered:

- Use of structural reinforcements (to increase foil strength, thus reducing the number of struts required to sustain the loads)
- Use of foil sweep (to maintain cavitation free flow on a thicker foil, thus increasing foil strength)
- Use of end-plates (to reduce induced drag)

Since the critical structural locations are in most cases at the foil-strut junctions, structural reinforcements (Fig. 17) were incorporated into the FE model. The reinforcements lead to improvements in L/D on the order of 15-20%, and thus, were added

in subsequent designs. The reinforcements, however, introduce additional structural design variables, which need to be adjusted for optimal structural arrangement and thus increase the structural design effort.

The use of sweep to increase foil thickness is discussed in Besnard et al. (1998) and only a brief summary is presented here. Under infinite swept foil conditions, sweep might be used to increase the cavitation onset speed of a foil, since, for a fixed foil, sweeping decreases flow acceleration on the foil, thus increasing the pressure. Equivalently, for the same cavitation speed, i.e. minimum pressure, the foil can be swept and its thickness increased. For example, for a cavitation index of about 0.27, the foil maximum thickness ratio can be increased from 0.06 (Fig. 9) to 0.066 by sweeping at 30 deg., and to 0.075 by sweeping at 45 deg. This increase in foil thickness, while generating the same lift coefficient, may be beneficial for structural purposes. When struts are added, since struts have to be streamlines, this benefit may be lost. It was shown in Besnard et al. (1998) that to answer this question it is necessary to perform a detailed design of the strut-foil junction. Since the detailed design is not addressed in the present study, sweep will not be considered.

Similarly, it was shown in Besnard et al. (1998) that end-plates can be used to decrease induced drag, and that for best results, the end-plates should extend downstream of the foil trailing edge and deeper than the foil tip. The improvements, however, are not drastic. Furthermore, the larger endplates would cause an increase in profile drag, thus leading to an even smaller improvement, or possibly to an increase, in total drag. Their use and design should be postponed to the detailed design phase.

3.2 L/D results and discussion

Results with structural reinforcements and a maximum allowable stress of 55 kpsi are presented here for various points in the design space. Table 1 presents a summary of the calculations performed. Results are presented for 75 and 90 knots at depth of 10 or 13 m. High, moderate, and low aspect ratios are considered. The foil maximum thickness ratio is usually chosen so that a reasonable lift coefficient can be attained at the given cavitation index (which depends on speed and depth as described in Sect. 2.2).

Test case S-1 can be thought of as an initial design. S-2 shows the effect of increased aspect ratio, from 10 for S-1 to 17 for S-2. A gain in L/D can be obtained with quarter skin friction coefficient. S-3 corresponds to placing the foil slightly deeper (13 m instead of 10 m) which allows increasing the foil thickness ratio from t/c = 0.06 to 0.08 for the same lift coefficient (0.29). An increase in L/D is observed. Other calculations were performed for greater depths, but strut bending moments increased and became critical, thus not allowing reducing the number of struts. The corresponding L/D was naturally lower. Finally, S-6 presents a test case where the aspect ratio is drastically reduced to 4. The foil chord and its thickness are increased. The resulting foil has higher strength and the strut requirements are therefore drastically reduced. The reduction in strut drag, however, is outweighed by the increase in induced drag.

When comparing results for 5000 tons at 75 kts and for the nominal skin friction coefficient, i.e. without skin friction reduction, L/D ratios are all very close to each other. Tradeoffs occur between strut profile drag and induced drag, i.e. a thicker wing (increased chord) comes at the expense of reduced aspect ratio. Foil profile drag remains essentially constant, its variations being due to Reynolds number variations. If skin friction drag reduction can be implemented, however, configurations with a greater aspect ratio will lead to better L/D values, as is obvious when comparing S-3 (L/D = 51 with quarter skin friction coefficient) and S-6 (L/D = 32).

Test cases S-4, S-5, and S-7 correspond to design variable variations for 90 kts. Similar observations to the 75 knot test cases can be made. At that speed, however, cavitation further reduces feasible foil thickness. Also, the dynamic pressure, which increases quadratically with speed, causes higher forces. The combination of both phenomena explains why the feasible L/D with quarter skin friction coefficient is reduced from 51 at 75 kts to 45 at 90 kts.

If the goal is to lift a total of 10000 tons, either two foils like S-3 are required, or the size of the foil system must be increased. The two-foil system would, in general, cause an increase in induced drag, which would reduce the overall L/D. In order to grasp what would occur if one were to lift 10,000 tons instead of 5,000 tons in a single foil, the foil span of test cases S-6 and S-7 is increased and test cases S-8 and S-9 are obtained. Due to the limit on the span at 65 m, the maximum aspect ratio achievable (approx. 8) does not reach as high values as for 5000 tons (approx. 17), and the resulting induced drag is greater, leading to a lower L/D ratio when skin friction drag reduction can be obtained.

CASE #	S-1	S-2	S-3	S-6	S-8	S-4	S-5	S-7	S-9
M (tons)	5000	5000	5000	5000	10000	5000	5000	5000	10000
V (kts)	75	75	75	75	75	90	90	90	90
d (m)	**10**	**10**	**13**	**10**	**10**	**13**	**13**	**13**	**13**
(t/c)	**.06**	**.06**	**.08**	**.06**	**.06**	**.06**	**.06**	**.06**	**.06**
AR	**10**	**17**	**17**	**4**	**8**	**16**	**10**	**4**	**8**
C_L	.290	.290	.292	.290	.290	.190	.190	.190	.190
c (m)	4.70	3.60	3.59	7.43	7.43	3.82	4.835	7.645	7.645
b (m)	46.97	61.24	61.08	29.71	59.42	61.16	48.35	30.58	61.16
C_{Di}	.0033	.0021	.0020	.0068	.0045	.0009	.0013	.0027	.0018
C_{Df}	.0053	.0055	.0059	.0050	.0050	.0053	.0051	.0048	.0048
$(L/D)_{foil}$	34	38	37	25	30	31	29	25	29
$\langle t/c \rangle_s$	.080	.080	.088	.080	.080	.063	.063	.063	.063
n_s	6	10	7	3	4	8	5	3	5
C_{Ds}	.0073	.00965	.00905	.0045	.0036	.0091	.0070	.0059	.0051
$(L/D)_{tot}$ @ c_f	**18**	**17**	**17**	**18**	**22**	**12**	**14**	**14**	**16**
BHP @ c_f	188	199	199	188	308	338	290	290	507
$(L/D)_{tot}$ @ .5	**30**	**30**	**31**	**25**	**33**	**24**	**26**	**24**	**28**
BHP@ .5	113	113	109	135	205	169	156	169	290
$(L/D)_t$ @ .25	**45**	**49**	**51**	**32**	**44**	**42**	**44**	**35**	**44**
BHP@ .25	75	69	66	106	154	94	92	116	185

Table 1. Results for single foil configurations

Results presented in this section show that, with quarter skin friction drag reduction, a L/D greater than 50 can be obtained for 60 kts, the goal of L/D = 50 is achievable for 75 kts, and, for 90 kts, L/D ratios around 45 can be reached. The corresponding break

horsepower requirements for 10,000 tons are less than 100 khp, around 130 khp, and less than 200 khp, respectively.

4 RESULTS FOR BIPLANE CONFIGURATIONS

The three components of total drag are (1) configuration induced drag, (2) foil profile drag, and (3) strut profile drag. Induced drag is due to lift and can be reduced mainly by increasing aspect ratio. Foil profile drag is mainly due to foil skin friction drag, which greatly depends on foil area, thus on lift coefficient. Since cavitation limits the range of feasible lift coefficients, the only avenue for drastically reducing total drag from the levels observed for the single foil configuration would be to find means of reducing the number of struts, or more generally, reducing the strut wetted area. For this purpose, a biplane arrangement, which as a whole should allow for improved structural integrity, is investigated. The biplane configuration is shown in Fig. 21. First, before L/D calculations can be carried out, both hydrodynamic and structural models have to be modified. These modifications are presented in Sects. 4.1 and 4.2, respectively. Sect. 4.3 presents the corresponding L/D results for two configurations.

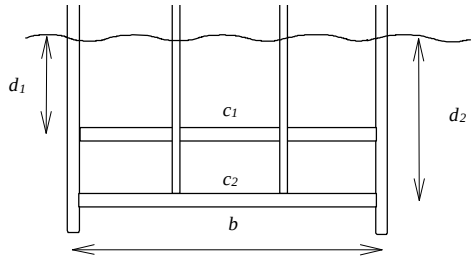

Figure 21. Biplane configuration.

4.1 Hydrodynamic interactions

When two foils are placed "close" to each other, they interact and the pressure distribution on the foils varies from that on foils, which do not interact. More specifically, the flow acceleration around the upper foil is increased and that the flow on for the lower foil is slightly decelerated when compared with the interaction-free case. In order to avoid cavitation on the upper foil, its thickness must be reduced. The reduction in upper foil thickness can actually be greater than 20%.

The consequences of the interaction are of primary importance for the upper foil since its thickness tends to drive the number of struts required for structural considerations. Another consequence of the interaction is that the lift coefficient for the upper foil is also reduced, which in turn requires a larger foil area to support the same mass at a given speed, thus adding wetted area and, therefore, profile drag.

This interaction is taken into account in the results presented below. Also, the induced drag calculation is performed for each test case using the Hess panel method for the modified configuration, in contrast with Sect. 3 where all results for induced drag are derived from Fig. 5.

4.2 Modifications in structural analysis

For the single foil configuration, the side load is centered at 60% depth on the struts. Since the biplane has two foil depths, this procedure has to be modified accordingly. The side loads applied to the biplane configuration are presented in Fig. 22. Δ_1 and Δ_2 are determined to satisfy the force and moment conservation equations. The continuous load is replaced by two point loads in the model, W_1 and W_2, placed at $\frac{2}{3}\ \Delta_1$ and $\frac{1}{2}\ \Delta_2$ as shown in Fig. 22. W_1 and W_2 correspond to the loads on the upper and lower foils, respectively.

The structural reinforcements discussed in Sect. 3.1 have also been included.

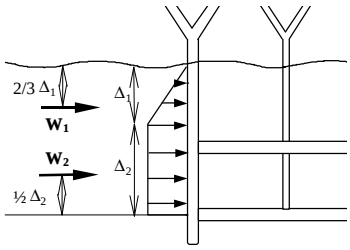

Figure 22. Side load model for the biplane configuration.

4.3 L/D results and discussion

Table 2 presents the results for two biplane configurations, one for 5000 tons and the other for 10000 tons, at 75 knots. The span of both upper and lower foils is the same, but their chord, constant for each foil, can be different. The depths considered are 9 m for the upper foil and 13 m for the lower foil.

For the test case B-1, the thickness ratio of the upper foil is a lot less than that of the lower foil because of the interaction and reduced cavitation index at the lesser depth. To compensate for the lower thickness ratio, a smaller aspect ratio for the upper foil is used, thus leading to a larger upper foil chord. This test case can be compared with test case S-1 of Sect. 3.2, even if deciding a proper test case for comparison is not straightforward. L/D results without skin friction reduction are of the same order as for the single foil. If quarter skin friction can be obtained, however, L/D results are less than for the single foil configuration, mainly due to a decrease in lift coefficient, other coefficients being almost constant. In particular, the strut drag coefficient is almost unchanged: the benefits of the biplane structural arrangement are cancelled by the reduction in foil thickness.

The second test case (B-2) can be compared with test case S-8 and is investigated to determine how lifting 10000 tons with two foils compares with lifting 10000 tons in one foil, taking advantage of all the span available (65m). The aspect ratio for the biplane configuration is higher, leading to a slightly lower induced drag coefficient. However, since the foil thickness is smaller (shorter chord), the foil strength is reduced and the number of struts goes from 4 for S-8 to 10 for B-2. Interestingly, the resulting L/D with quarter skin friction drag remains unchanged (44 vs. 43).

In conclusion, from the test cases considered, even if the biplane configuration does not seem to be worse than the single foil configuration, it does not seem to offer significant advantages either. The benefits of the structural arrangement are traded for reduced foil thickness and therefore more struts leading to an increase in strut drag. A deeper investigation might is necessary to determine if a different strut arrangement would yield better results.

Case #	B-1	B-2
M (tons)	5000	10000
V (kts)	75	75
d_1, d_2 (m)	**9, 13**	**9, 13**
$(t/c)_1$, $(t/c)_2$	**.05, .09**	**.06, .08**
AR_1, AR_2	**10.7, 15.4**	**16, 16**
C'_{L1}, C'_{L2}	.21, .29	.18, .33
C_L	.247	.255
c_1, c_2 (m)	3.80, 2.64	3.96, 3.96
b (m)	40.7	63.3
C_{Di}	***.00293***	***.00296***
C_{Df}	***.00575***	***.0056***
$(L/D)_{foil}$	28	30
$<t/c>_s$	.083	.083
n_s	7	10
C_{Ds}	***.00693***	***.00605***
$(L/D)_{tot}$ @ c_f	**16**	**17**
BHP @ c_f	211	398
$(L/D)_{tot}$ @ .5	**27**	**29**
BHP@ .5	125	233
$(L/D)_t$ @ .25	**40**	**43**
BHP@ .25	85	157

Table 2. Results for biplane configurations

5 CONCLUSION

The paper studies the feasibility of a hydrofoil-based fast ship concept to reduce drastically sea lift transit times to remote locations by reaching cruise speeds around 100 knots. The essential factor in attaining a range of at least 10,000 nautical miles is the determination of the maximum practical lift to drag ratio (L/D), consistent with the desired high speed limits set by cavitation onset and structural considerations.

The paper presents a multi-disciplinary design/optimization method which integrates both structural (ability to carry the loads) and hydrodynamic (cavitation free flow) aspects. The approach is used to determine the maximum achievable lift-to-drag ratio (hopefully larger than 50) of an isolated foil-strut arrangement at high transit speeds (greater than 75 knots) while lifting masses of 5,000 or 10,000 tons.

It concentrates on a single lifting surface carrying up to 10,000 metric tons of mass above the sea surface and having a maximum span of 65 meters. Stability and control are not investigated here.

First, the tools necessary for the study are presented. They comprise a panel method to compute three-dimensional flows around arbitrary configurations, a foil cross-section optimization tool, a strut cross-section design tool, and a structural analysis tool. High Froude number free surface flows are modeled with a negative image in the Hess higher-order panel method. Induced drag is calculated in the far field. The foil cross-section optimization tool is composed of an optimizer, a Computational Fluid Dynamics code, and a program that creates general shapes. It is used to design foil cross-sections which, for a prescribed maximum thickness, produce the highest lift coefficient possible without causing any cavitation or flow separation. The profile drag is calculated within the Computational Fluid Dynamics module of the tool. The structural analysis tool is composed of a Finite Element model generator that generates the model automatically and prepares the input data for the Finite Element method.

At fixed transit speed and for a given mass to lift, the design approach consists of identifying the appropriate design variables (DV's), selecting their value, and calculating the corresponding drag using the tools previously described. Then these DV's are varied to reduce drag. Appropriate DV's are the depth, the foil thickness ratio and the aspect ratio. For a given depth and thickness ratio, the shape of the foil cross-section is determined with the optimization tool and the section lift and profile drag coefficients are calculated. The foil area can then be determined from the mass to lift, and the chord and span of the foil are found from the selected aspect ratio. The induced drag can then be calculated with the panel method, assuming that there are struts at the tips of the foil. Finally, structural analysis is performed to determine the number of struts needed to sustain the calculated loads for that configuration. The total drag coefficient is then obtained by adding induced drag to the foil and strut profile drag. Design variables can then be varied to improve the design, i.e. to reduce drag. The design approach is general and can be implemented into a general optimization procedure.

Results are first presented for a single foil configuration. Preliminary results showed that modifications to the design needed to be made in order to reach L/D greater than 50. The effects of foil sweep (to increase foil thickness), structural reinforcements (to increase local strength), and endplates (to reduce induced drag) are analyzed. Structural reinforcements show great benefits and are incorporated in all subsequent designs. Several points in the design space are analyzed for speeds of 75 and 90 knots, and masses of 5000 and 10000 tons. Results show a rather small dependency of the design parameters on L/D, suggesting that drastic improvements can not be obtained by conducting extensive parametric studies or implementing a general optimization procedure.

A biplane configuration is investigated to determine whether a more sound structural arrangement could lead to a substantial reduction in the number of struts. Preliminary results indicate that similar L/D results should be expected for this type of arrangement when comparing with the single foil configuration.

The results show that, if means of reducing the skin friction to a quarter of its nominal value are devised, the goal of L/D = 50 is achievable for 75 knots and, for 90 knots, L/D ratios around 45 can be reached. The corresponding break horsepower requirements for 10,000 tons are around 130 khp and less than 200 khp, respectively.

Several avenues could be investigated to further reduce drag. As previously discussed, the design process exposed herein could be implemented automatically and incorporated into an optimization loop. Also, other types of structural arrangements could be analyzed in order to minimize the strut wetted area. Other areas of improvements include (but are not limited to) hydrofoil cross-section optimization for drag, use and optimization of a more detailed structural layout (including spars, ribs and skin), structural and hydrodynamic design of the foil/strut junction, use of foil sweep, and use of end-plates.

6 ACKNOWLEDGEMENTS

The financial support of DARPA through an ONR grant (nb. N00014-97-1-0964) is gratefully acknowledged. Also, the authors would like to recognize John Hess for his contribution to the present study.

REFERENCES

Abbott, I.H. and Von Doenhoff, A.E., 1959, *Theory of Wing Sections*, Dover Publications, Inc., NY.

Besnard, E., Schmitz, A., Boscher, E., Garcia, N., and Cebeci, T., 1998, " Two-Dimensional Aircraft High Lift System Design and Optimization," Paper No. 98-0123.

Besnard, E., Schmitz, A., Tzong, G., Kaups, K., Hefazi, H., Hess, J., Chen, H.H., and Cebeci, T., 1998, "Hydrofoil design and optimization for fast ships," Report AE-98-1, Aerospace Engineering Department, California State University, Long Beach.

Cebeci, T., 1998, *An Engineering Approach to the Calculation of Aerodynamic Flows*, to be published.

Cebeci, T., Besnard, E. and Chen, H.H., 1996, "Calculation of Multi-element Airfoil Flows, Including Flap Wells," AIAA Paper No. 96-0056.

Durand, W.F., 1934, *Aerodynamic Theory*, Vol II, Section E.III.B, Julius Springer, Ed.

Eyi S., 1995, "Performance Evaluation and Improvements of CFD-based Aerodynamic Design Optimization", Ph.D. Dissertation, University of Illinois, Urbana Champaign.

Hicks, R., and Henne, P., 1978, "Wing Design by Numerical Optimization," *J. Aircraft*, Vol. 15, No. 7, pp. 407-413, July 1978.

Hess, J.L., 1974, "The problem of three-dimensional lifting flow and its solution by means of surface singularity distribution," *Comp. Meth. in Appl. Mech. and Eng*., Vol 4, 1974; also McDonnell Douglas Report No. MDC J5679, 1972.

Hess, J.L., Firedman D.M., and Clark, R.W., 1985, "Calculation of compressible flow about three-dimensional inlets with auxiliary inlets, slats and vanes by means of a panel method," McDonnell Douglas Report No. MDC J3789, 1985; also NASA CR-174975 and AIAA Paper No. AIAA-85-1196.

Squire, H.B., and Young, A. D., 1938, *The calculation of the profile drag of aerofoils*, ARC RM 1838.

Vanderplaats, Miura & Associates, Inc., 1994, "DOT Users Manual, Version 4.10," VMA Engineering, ©1994.